

Squeeze-and-Attention Networks for Semantic Segmentation

Zilong Zhong, Zhong Qiu Lin, Rene Bidart, Xiaodan Hu, Ibrahim Ben Daya, Jonathan Li, Alexander Wong
 University of Waterloo, Waterloo, ON, Canada

Abstract

Squeeze-and-excitation (SE) module enhances the representational power of convolution layers by adaptively re-calibrating channel-wise feature responses. However, the limitation of SE in terms of attention characterization lies in the loss of spatial information cues, making it less well suited for perception tasks with very high spatial inter-dependencies such as semantic segmentation. In this paper, we propose a novel squeeze-and-attention network (SANet) architecture that leverages a simple but effective squeeze-and-attention (SA) module to account for two distinctive characteristics of segmentation: i) pixel-group attention, and ii) pixel-wise prediction. Specifically, the proposed SA modules impose pixel-group attention on conventional convolution by introducing an ‘attention’ convolutional channel, thus taking into account spatial-channel inter-dependencies in an efficient manner. The final segmentation results are produced by merging outputs from four hierarchical stages of a SANet to integrate multi-scale contexts for obtaining enhanced pixel-wise prediction. Empirical experiments using two challenging public datasets validate the effectiveness of the proposed SANets, which achieved 83.2% mIoU (without COCO pre-training) on PASCAL VOC and a state-of-the-art mIoU of 54.4% on PASCAL Context.

1. Introduction

Semantic segmentation, also known as scene parsing, involves three levels of task: image-level categorical recognition, pixel-level dense prediction, and pixel-group attention modeling. As illustrated in Fig. 1, semantic segmentation and image classification are closely related in that they share the objective of image level recognition but segmentation includes two other levels of dense prediction and pixel grouping. Previous segmentation works mainly focus on improving segmentation performance from the pixel-level but largely ignore the pixel-group attention [26, 5, 41, 40, 4, 3]. In the following paragraphs, we discuss semantic segmentation from the perspective of these three task levels.

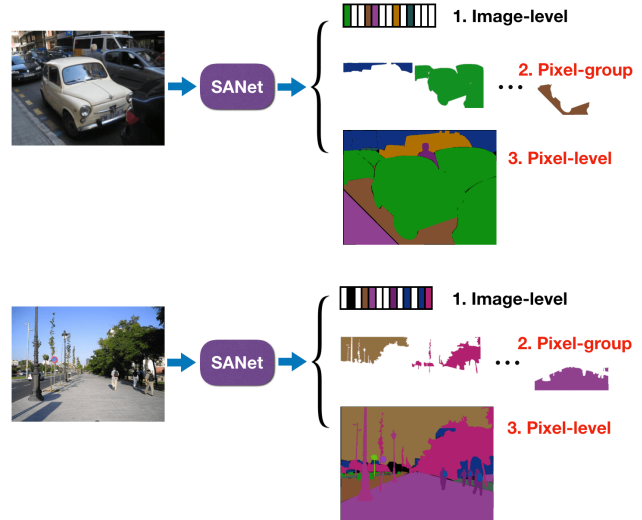


Figure 1: Semantic segmentation can be disentangled into three tasks: image-level categorization, pixel-group attention, and pixel-level dense prediction. The first task is shared with image classification and the latter two are specific for segmentation. Inspired by the success of squeeze-and-attention net (SENet) for classification, we design a novel squeeze-and-attention net (SANet) to improve the performance of dense prediction and account for the largely ignored pixel-group attention.

Image-level categorical recognition is useful for both semantic segmentation and image classification, and this similarity enables the network backbones pre-trained for classification to be easily extended to semantic segmentation via replacing classification heads with segmentation heads. This approach derives from the Fully convolutional network (FCN) [26] for dense pixel-wise prediction and we have witnessed that FCN-based models significantly improve segmentation performance in multiple benchmarks [15, 11, 2, 23, 7, 41, 5].

In contrast to image classification semantic segmentation requires dense pixel-wise prediction, so recent works have come up with multiple approaches to extend standard clas-

sification networks to perform better for dense prediction. For example, pooling methods and dilated convolution are utilized to boost segmentation performance. Pooling-based modules are widely used to aggregate spatial information from different scales, like the pyramid pooling module [41] and atrous spatial pyramid pooling [5]. Also, atrous convolution are used to enlarge the receptive scales of convolutional kernels to improve segmentation performance [8]. Although atrous convolution and multi-scale pyramid pooling have been proved effective for semantic segmentation, existing methods have mainly used pooling layers for enhancing the output of the last stage of backbone networks, not throughout the entire backbone network. With the introduction of skip connections [16], low-level features are fused with high-level features to encourage more accurate boundaries[31]. Although these methods achieved promising results in segmentation benchmarks, the non-adaptive multi-scale feature learning modules hinder the generality of these methods and they have not taken advantage of the multi-stage outputs of backbone networks.

Semantic segmentation implicitly facilitates pixel-group attention modeling through grouping pixels with different semantic meaning. Given the effectiveness of SE module for image classification, we put forward a hypothesis: *There exists a module that specifically accounts for pixel-level prediction and pixel-group attention.* If this hypothesis is correct, this module should emphasize the spatial information that SE modules omit. Additionally, it should have a simple yet effective architecture like its counterpart for classification. Therefore, inspired by the effectiveness of SE module for image classification [18], we design a novel squeeze-and-attention (SA) module with a down-sampled but not fully squeezed convolutional channel to produce a flexible module. The SA module adapts the SE module from classification to segmentation and it takes a dual-usage mechanism on the down-sampled attention channel. Specifically, this additional channel generates categorical specific soft attention masks for pixel grouping, while adding scaled spatial features on top of the classical convolution channels for pixel-level prediction. In other words, the output of the down-sampled attention channel functions as both global attention masks and multi-scale contextual features simultaneously.

To take advantage of multi-scale features of backbone networks, we design a SA net (SANet) built on top of SA modules to merge their multi-stage outputs, resulting in better object boundaries and hence better scene parsing outcomes. 2D Convolution can be used to generate attention masks because each convolutional kernel sweeps across input feature maps. The spatial attention mechanism introduced by the SA modules emphasizes the attention of pixel groups that belong to the same classes at different spatial scales. Additionally, the squeezed channel works as global

attention masks. This simple but effective innovation makes it easier to generalize SANets to other related visual recognition tasks. We validate the SANets using three challenging segmentation datasets: PASCAL context and PASCAL VOC 2012 [11, 45, 44].

The contributions of this paper are three-fold:

- We disentangle semantic segmentation into three tasks: image-level categorization, pixel-level dense prediction, and pixel-group attention.
- We design a squeeze-and-attention (SA) module that adapts SE modules for semantic segmentation via accounting for the multi-scale dense prediction of individual pixels and the spatial attention of pixel groups.
- We propose a squeeze-and-attention network (SANet) with multi-level heads to exploit the representational boost from SA modules, and to integrate multi-scale contextual features and image-level categorical information.

2. Related Works

Multi-scale contexts. Recent improvements for semantic segmentation have mostly been made possible by incorporating multi-scale contextual features to facilitate segmentation models to extract discriminative features. A Laplacian pyramid structure is introduced to combine multi-scale features[14] introduced. A multi-path RefineNet explicitly integrate features extracted from multi-scale inputs to boost segmentation outputs. Encoder-decoder architectures have been used to fuse features that have different levels of semantic meaning [2, 29]. The most popular methods adopt pooling operations to collect spatial information from different scales [41, 5]. Similarly, EncNet employs an encoding module that projects different contexts in a Gaussian kernel space to encode multi-scale contextual features [40]. Graphical models like CRF and MRF are used to impose smoothness constraints to obtain better segmentation results [43, 24, 1]. Recently, a gather-excite module is designed to alleviate the local feature constraints of classic convolution by gathering features from long-range contexts [17]. We improve the multi-scale dense prediction by merging outputs from different stages of backbone residual networks.

Channel-wise attention. Selectively weighting the channels of feature maps effectively increases the representational power of conventional residual modules. A good example is the squeeze-and-excitation (SE) module because it emphasizes attention on the selected channels of feature maps. This module significantly improves classification accuracy of residual networks by grouping related classes together [18]. EncNet also uses the categorical recognition capacity of SE modules [40]. Discriminative Feature Network (DFN) utilize the channel-weighting paradigm in its

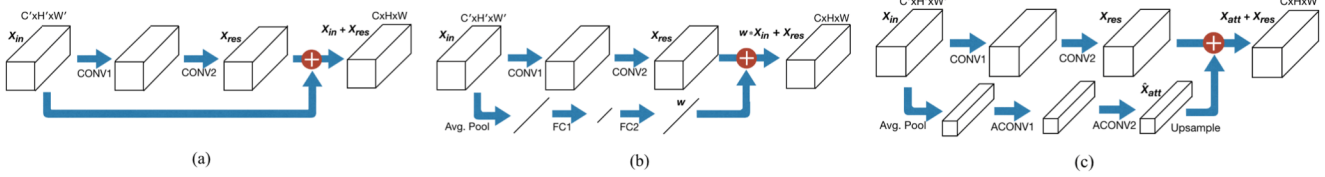


Figure 2: (a) Residual Block; (b) Squeeze-and-excitation (SE) module; (c) Squeeze-and-attention (SA) module; and For simplicity, we show convolution (CONV), fully connected (FC), average (Avg. Pool) and max pooling (Max Pool) layers, while omitting normalization and activation layers. The SA module has a similar structure as the SE module that contains an additional path to learn weights for re-calibrating channels of output feature maps X_{out} . The difference lies in that the attention channel of SA modules uses max pooling to down sample feature maps but not fully squeeze as in the SE modules. Therefore, we term this channel the attention convolution (ACONV) channel.

smooth sub-network. [20]. Also, in this work, we use the SE module for the task of categorical information to boost segmentation performance.

Pixel-group attention. The success of attention mechanism in neural language processing foster its adoption for semantic segmentation. Spatial Transform Networks explicitly learn spatial attention in the form of affine transformation to increase feature invariance [19]. Since machine translation and image translation share many similarities, RNN and LSTM have been used for semantic segmentation by connecting semantic labeling to translation [43, 20]. [7] employed a scale-sensitive attention strategy to enable networks to focus on objects of different scales. [42] designed a specific spatial attention propagation mechanism, including a collection channel and a diffusion channel. [36] used self-attention masks by computing correlation metrics. [17] designed a gather-and-excite operation via collecting local features to generate hard masks for image classification. Different from exiting attention modules, we use the down-sampled channels that implemented by pooling layers to aggregate multi-scale features and generate soft global attention masks simultaneously. Therefore, the SA models enhance the objective of pixel-level dense prediction and consider the pixel-group attention that has largely been ignored.

3. Framework

Classical convolution mainly focuses on spatial local feature encoding and Squeeze-and-Excitation (SE) modules enhance it by selectively re-weighting feature map channels through the use of global image information[18]. Inspired by this simple but effective SE module for image-level categorization, we design a Squeeze-and-Attention (SA) module that incorporates the advantages of fully convolutional layers for dense pixel-wise prediction and additionally adds an alternative, more local form of feature map re-weighting, which we call pixel-group attention. Similar to the SE mod-

ule that boosts classification performance, the SA module is designed specifically for improving segmentation results.

3.1. Residual Block Formulation

Residual networks (ResNets) are widely used as the backbones of segmentation networks because of their strong performance on image recognition, and it has been shown that ResNets pre-trained on the large image dataset ImageNet transfer well to other vision tasks, including semantic segmentation [41, 5]. Since classical convolution can be regarded as a spatial attention mechanism, we start from the residual blocks that perform as the fundamental components of ResNets. As shown in Fig. 2 (a), conventional residual blocks can be formulated as:

$$\mathbf{X}_{out} = \mathbf{X}_{in} + \mathbf{X}_{res} = \mathbf{X}_{in} + F(\mathbf{X}_{in}; \Theta, \Omega) \quad (1)$$

where $F(\cdot)$ represents the residual function, which is parameterized by Θ and Ω denotes the structure of two convolutional layers. $\mathbf{X}_{in} \in \mathbb{R}^{C' \times H' \times W'}$ and $\mathbf{X}_{out} \in \mathbb{R}^{C \times H \times W}$ are input and output feature maps. The SE module improve residual block by re-calibrating feature map channels, It is worth noting that we adopt the updated version of SE module, which perform equivalently to original one in [18]. As shown in Fig. 2 (b), the SE module can be formulated as:

$$\mathbf{X}_{out} = w * \mathbf{X}_{in} + F(\mathbf{X}_{in}; \Theta, \Omega) \quad (2)$$

where the learned weights w for re-calibrating the channels of input feature map \mathbf{X}_{in} is calculated as:

$$w = \Phi(W_2 * \sigma(W_1 * APool(\mathbf{X}_{in}))), \quad (3)$$

where the $\Phi(\cdot)$ represents the sigmoid function and $\sigma(\cdot)$ denotes the ReLU activation function. First, an average pooling layer is used to ‘squeeze’ input feature map \mathbf{X}_{in} . Then, two fully connected layers parameterized by W_1 and W_2 are adopted to get the ‘excitation’ weights. By adding such a

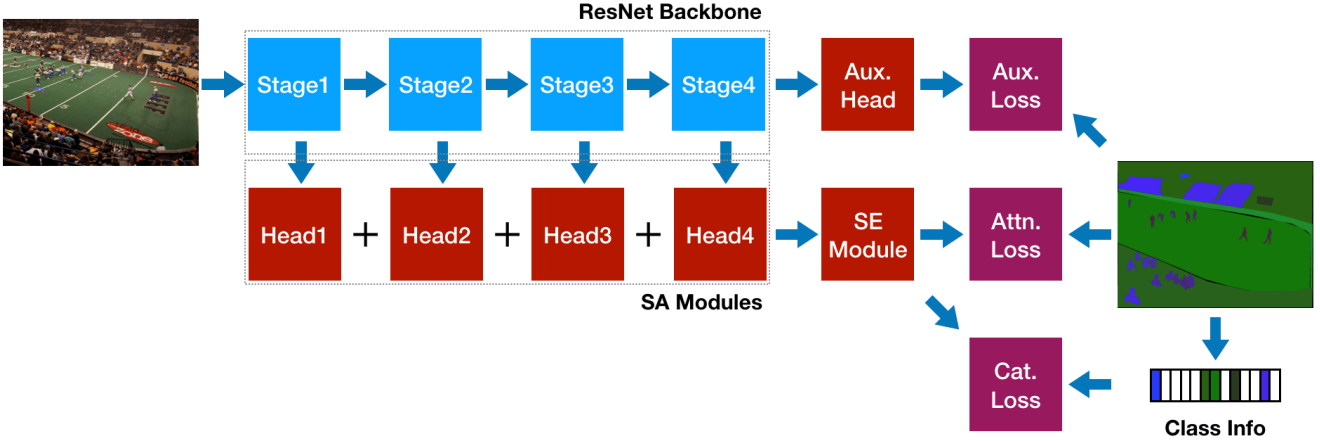


Figure 3: Squeeze-and-attention Network. The SANet aggregates outputs from multiple hierarchical SA heads to integrate multi-scale features instead of extracting them from the last stage. To regularize the training process, in addition to the attention loss, we employ two losses to take image-level categorization and pixel-level dense prediction into consideration. The auxiliary head designed for auxiliary loss is composed of fully convolutional layers. The SE head designed for categorical loss has a structure of a SE module. In this way, we utilize the pixel-group attention extraction capacity of SA modules and integrate multi-scale contextual features simultaneously.

simple re-weighting mechanism, the SE module effectively increases the representational capacity of residual blocks.

3.2. Squeeze-and-attention modules

Useful representation for semantic segmentation appears at both global and local levels of an image. At the pixel level, convolution layers generate feature maps conditional on local information, as convolution is computed locally around each pixel. Pixel level convolution lays the foundation of all semantic segmentation modules, and increased receptive field of convolution layers in various ways boost segmentation performance [41, 40], showing larger context is useful for semantic segmentation.

At the global image level, context can be exploited to determine which parts of feature maps are activated, because the contextual features indicate which classes likely to appear together in the image. Also, [40] shows that the global context provides a broader field of view which is beneficial for semantic segmentation. Global context features encode these areas holistically, rather than learning a re-weighting independently for each portion of the image. However, there remains little investigation into encoding context at a more fine-grained scale, which is needed because different sections of the same image could contain totally different environments.

To this end, we design a squeeze-and-attention (SA) module to learn more representative features for the task of semantic segmentation through a re-weighting mechanism that accounts for both local and global aspects. The SA module expands the re-weighting channel of SE module,

as shown in figure 2 (b), with spatial information not fully squeezed to adapt the SE modules for scene parsing. Therefore, as shown in Fig. 2 (c), a simple squeeze-attention module is proposed and can be formulated as:

$$\begin{aligned} \mathbf{X}_{out} &= \mathbf{X}_{attn} + \mathbf{X}_{res} \\ &= Up(\sigma(\hat{\mathbf{X}}_{attn})) + F(\mathbf{X}_{in}; \Theta, \Omega) \end{aligned} \quad (4)$$

where $Up(\cdot)$ is a up-sampled function to expand the output of the attention channel:

$$\hat{\mathbf{X}}_{attn} = F_{attn}(MPool(\mathbf{X}_{in}); \Theta_{attn}, \Omega_{attn}) \quad (5)$$

where $\hat{\mathbf{X}}_{attn}$ represents the output of the attention convolution channel $F_{attn}(\cdot)$, which is parameterized by Θ_{attn} and the structure of attention convolution layers Ω_{attn} . A max pooling layer $MPool(\cdot)$ is used to perform the not-fully-squeezed operation and then the output of the attention channel $\hat{\mathbf{X}}_{attn}$ is up-sampled to match the output of main convolution channel \mathbf{X}_{res} .

In this way, the SA modules extend SE modules with preserved spatial information and the up-sampled output of the attention channel \mathbf{X}_{attn} aggregates non-local extracted features upon the main channel.

3.3. Squeeze-and-attention network

We build a SA network (SANet) for semantic segmentation on top of the SA modules. Specifically, we use SA modules as heads to extract features from the four stages

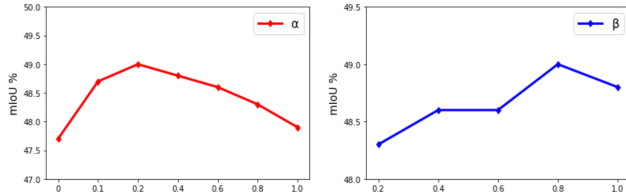


Figure 4: Ablation study of α and β that weight the categorical loss and auxiliary loss, respectively. We test SANets using ResNet50 as backbones and train 20 epochs for each case. Left: mIoUs of SANets with fixed $\beta = 0.8$ for selecting α . Right mIoUs of SANets with fixed $\alpha = 0.2$ for selecting β .

SANet	Main	Attention	Output
SA Head1	128×128	16×16	128×128
SA Head2	64×64	8×8	64×64
SA Head3	64×64	8×8	64×64
SA Head4	64×64	8×8	64×64
SE Head	64×64	—	64×64
Aux Head	64×64	—	64×64

Table 1: Architecture of a SANet with four SA heads on PASCAL Context. All convolution layers of SANets adopt two dimensional 3×3 kernels. Empirically, the down-sample and up-sample ratio of attention channels is set to 8. Suppose that the input image has a size of $3 \times 512 \times 512$, the feature map sizes of the inputs, main channels (Main), attention channels (Attention), and outputs of SA heads are papered, along with those of the SE module and the auxiliary head.

of backbone networks to fully exploit their multi-scale. As illustrated in Fig. 3, we consider the three-level tasks of semantic semantic segmentation and use three corresponding losses: categorical loss (Cat. loss) for image-level categorization, auxiliary loss (Aux. loss) for pixel-wise dense prediction, and attention loss (Attn. loss) for pixel-group attention. Therefore, the total loss of SANets can be represented as:

$$L_{SANet} = L_{Attn} + \alpha * L_{Cat} + \beta * L_{Aux} \quad (6)$$

where α and β are weighting parameters of categorical loss and auxiliary loss, respectively. Each component of the total loss can be formulated as follows:

$$L_{Attn} = \frac{1}{N \times M} \sum_{n=1}^N \sum_{i=1}^M \sum_{j=1}^C Y_{nij} \log \hat{Y}_{nij}^{Attn} \quad (7)$$

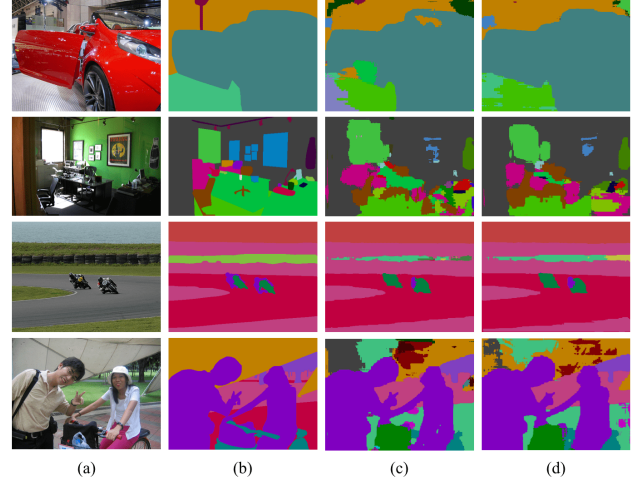


Figure 5: Example of semantic segmentation results on PASCAL Context validation set. Example of semantic segmentation results on PASCAL VOC validation set. (a) Raw images. (b) Groud truth images. (c) Results of a FCN baseline. (d) Results of a SANet. SANet generates more accurate results, especially for object boundaries. The last raw shows a failed example with relative complex contexts, which bring challenges for segmentation models.

$$L_{Cat} = \frac{1}{N} \sum_{n=1}^N \sum_{j=1}^C y_{nj} \log \hat{y}_{nj}^{Cat} + (1 - y_{nj}) \log (1 - \hat{y}_{nj}^{Cat}) \quad (8)$$

$$L_{Aux} = \frac{1}{N \times M} \sum_{n=1}^N \sum_{i=1}^M \sum_{j=1}^C Y_{nij} \log \hat{Y}_{nij}^{Aux} \quad (9)$$

where N is number of training data size for each epoch, M represents the spaital locations, and C denotes the number of classes for a dataset. \hat{Y}_{nij} and Y_{nij} are the predictions of SANets and ground truth, \hat{y}_{nj} and y_{nj} are the categorical predictions and targets to calculate the categorical loss L_{Cat} . The L_{Cat} takes a binary cross entropy form. L_{Attn} and L_{Aux} are typical cross entropy losses. The auxiliary head is similar to the strategy of deep supervision [41, 40], but its input comes from the fourth stage of backbone ResNet instead of the commonly used third stage. The final prediction of SANets integrates the outputs of multiple SA heads and is regularized by a SE head. Hence, the final segmentation prediction of a SANet is:

$$\hat{Y} = \hat{y}^{Cat} * \hat{Y}^{Attn} + \hat{Y}^{Attn} \quad (10)$$

Dilated FCNs have been used as the backbones of SANets. Suppose that the input image has a size of $3 \times 512 \times 512$; Table 1 shows the detailed feature map sizes of SA heads, along with those of a SE module and an auxiliary head. The main channel of SA modules has the same channel numbers as their attention counterparts and the same

Model	Backbone	SA	Cat	Aux	PAcc	mIoU
FCN	Res50				74.5	43.2
SANet	Res50	✓			77.2	49.2
SANet	Res50	✓	✓		79.0	50.7
SANet	Res50	✓	✓	✓	79.3	51.9
SANet	Res101	✓	✓	✓	80.6	53.0
SANet	EffNet-b7	✓	✓	✓	81.6	55.3

Table 2: Ablation study results of SANets on PASCAL Context dataset (59 classes without background). SA: Squeeze-and-attention heads. Cat: Categorical loss. Aux: Auxiliary Loss. PAcc: Pixel accuracy (%). mIoU: Mean intersection of union (%).

spatial sizes as the input features. All convolution layers of SANets adopt 2D 3×3 kernels. Empirically, we reduce the channel sizes of inputs to a fourth in both main and attention channels, set the downsample (max pooling) and upsample ratio of attention channels to 8, and set the channel number of the intermediate fully connected layer of SE modules to 4 in both datasets. We add a convolutional layer to adapt outputs of SA heads to the class number of PASCAL Context dataset. Therefore, the outputs of all SA heads have a depth of 59. To merge the outputs of four SA heads, we upsample the outputs of SA head2-4 to a spatial size of 128×128 in order to match that of SA head1.

4. Experimental Results

In this section, we first compare SA module to SE modules, then conduct an ablation study using the PASCAL Context [28] dataset to test the effectiveness of each component of the total training loss, and further validate SANets on the challenging PASCAL VOC dataset [12]. Following the convention for scene parsing [5, 40], we paper both mean intersection and union (mIoU) and pixel-wise accuracy (PAcc) on PASCAL Context, and mIoU only on PASCAL VOC dataset to assess the effectiveness of segmentation models.

4.1. Implementation

We use Pytorch [30] to implement SANets and conduct ablation studies. For the training process, we adopt a poly learning rate decreasing schedule as in previous works [41, 40]. The starting learning rates for PASCAL Context and PASCAL VOC are 0.001 and 0.0001, respectively. Stochastic gradient descent and poly learning rate annealing schedule are adopted for both datasets. For PASCAL Context dataset, we train SANets for 40 epochs. As for the PASCAL VOC dataset, we pretrain models on the COCO dataset. Then, we train networks for 50 epochs on the validation set. We adopt the ResNet50 and ResNet101 as the

Model	Backbone	mIoU
FCN [26]		37.8
CRF-RNN[43]		39.3
ParseNet[24]		40.4
BoxSup[10]		40.5
HighOrder-CRF[1]		41.3
Piecewise[22]		43.3
Deeplab-v2[5]	ResNet101	45.7
RefineNet[21]	ResNet152	47.3
EncNet[40]	ResNet101	51.7
SANet (ours)	ResNet101	52.1
SANet (ours)	EffNet-b7	54.4

Table 3: Mean intersection over union (%) results on PASCAL Context dataset (60 classes with background).

Model	PAcc	mIoU
FCN50	76.2	44.9
FCN101	76.7	45.6
FCN50-SE	76.0	44.6
FCN101-SE	76.6	45.7
SANet50	78.9	49.0
SANet101	79.2	50.1

Table 4: Pixel accuracy (PAcc) and mIoUs of baseline dilated FCNs, dilated FCNs with SE modules (FCN-SE), and SANets using ResNet50 or ResNet101 as backbones on PASCAL Context. SANet significantly output their SE counterparts and baseline models. Each model is trained for 20 epochs

backbones of SANets because these networks have been widely used for mainstream segmentation benchmarks. We set the batch-size to 16 in all training cases and use sync batch normalization across multiple gpus recently implemented by [40]. We use four SA heads to exploit the multi-scale features of different stages of backbones and also to regularize deep networks.

4.2. Results on PASCAL Context

The Pascal Context dataset contains 59 classes, 4998 training images, and 5105 test images. Since this dataset is relatively small in size, we use it as the benchmark to design module architectures and select hyper-parameters including α and β . To conduct an ablation study, we explore each component of SA modules that contribute to enhancing the segmentation results of SANets.

The ablation study includes three parts. First, we test the impacts of the weights α and β of the total training loss. As shown in Fig. 4, we test α from 0 to 1.0, and find that

the SANet with $\alpha = 0.2$ works the best. Similarly, we fix $\alpha = 0.2$ to find that $\beta = 0.8$ yields the best segmentation performance. Second, we study the impacts of categorical loss and auxiliary loss of in equation (7) using selected hyper-parameters. Table 2 shows that the SANet, which contains the four dual-usage SA modules, using ResNet50 as the backbone improves significantly (a 2.7% PAcc and 6.0% mIoU increase) compared to the FCN baseline. Also, the categorical loss and auxiliary loss boost the segmentation performance.

We compare SANets with state-of-the-art models to validate their effectiveness, as shown in Table 3, the SANet using ResNet101 as its backbone achieves 53.0% mIoU. The mIoU equals to 52.1% when including the background class this result and outperforms other competitors. Also, we use the recently published Efficient Net (EffNet) [33] as backbones. Then, the EffNet version SANet achieved state-of-the-art 54.4% mIoU that sets new records for the PASCAL Context dataset. Fig. 4 shows the segmentation results of a ResNet50 FCN and a SANet using the same backbone. In the first three rows, SANets generate better object boundaries and higher segmentation accuracy. However, for complex images like the last row, both models fail to generate clean parsing results. In general, the qualitative assessment is in line with quantitative papers.

We also validate the effectiveness of SA modules by comparing them with SE modules on top of the baseline dilated FCNs, including ResNet50 and ResNet101. Table 4 shows that the SANets achieve the best accuracy with significant improvement (4.1% and 4.5% mIoU increase) in both settings, while FCN-SE models barely improve the segmentation results.

4.3. Attention and Feature Maps

The classic convolution already yields inherent global attention because each convolutional kernel sweeps across spatial locations over input feature maps. Therefore, we visualize the attention and feature maps of a example of PASCAL VOC set and conduct a comparison between Head1 and Head4 within a SANet To better understand the effect of attention channels in SA modules. We use L2 distance to show the attention maps of the attention channel within SA module, and select the most activated feature map channels for the outputs of the main channel within the same SA module. The activated areas (red color) of the output feature maps of SA modules can be regarded as the pixel groups of selected points. For the sake of visualization, we scale all feature maps illustrated in Figure 6 to the same size. we select three points (red, blue, and magenta) in this examples to show that the attention channel emphasizes the pixel-group attention, which is complementary to the main channels of SA modules that focus on pixel-level prediction.

Interestingly, as shown in Figure 6, the attention chan-

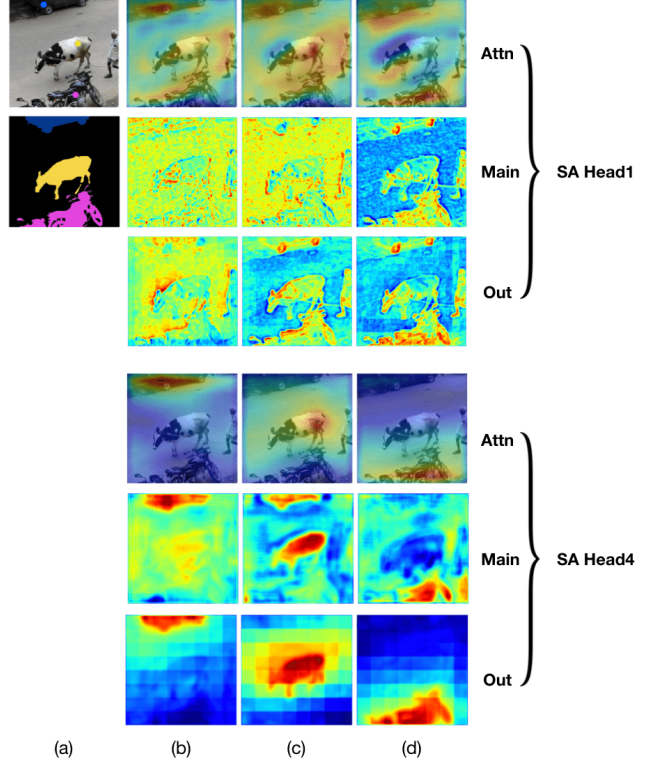


Figure 6: Attention and feature map visualization of SA head1 and head4 of a trained SANet on PASCAL VOC dataset. For each head, the feature maps of main channel, attention channel, and output are demonstrated. (a) Raw image and its ground truth; visualization results of (b) blue point; (c) yellow point; and (d) magenta point.

nels in low-level (SA head1) and high-level (SA head4) play different roles. For the low-level stage, the attention maps of the attention channel have broad field of view, and feature maps of the main channel focus on local feature extraction with object boundary being preserved. In contrast, for the high-level stage, the attention maps of the attention channel mainly focus on the areas surrounding selected points, and feature maps of the main channel present more homogeneous with clearer semantic meaning than those of head1.

4.4. Results on PASCAL VOC

The PASCAL VOC dataset [12] is the most widely studied segmentation benchmark, which contains 20 classes and is composed of 10582 training images, and 1449 validation images, 1456 test images. We train the SANet using augmented data for 80 epochs as previous works [26, 10].

First, we test the SANet without COCO pretraining. As shown in Table 5, the SANet achieves 83.2% mIoU which is higher than its competitors and dominates multiple classes, including aeroplane, chair, cow, table, dog, plant, sheep,

Method	aero	bike	bird	boat	bottle	bus	car	cat	chair	cow	table	dog	mIoU
FCN [26]	76.8	34.2	68.9	49.4	60.3	75.3	74.7	77.6	21.4	62.5	46.8	71.8	62.2
DeepLabv2 [5]	84.4	54.5	81.5	63.6	65.9	85.1	79.1	83.4	30.7	74.1	59.8	79.0	71.6
CRF-RNN [43]	87.5	39.0	79.7	64.2	68.3	87.6	80.0	84.4	30.4	78.2	60.4	80.5	72.0
DeconvNet [29]	89.9	39.3	79.7	63.9	68.2	87.4	81.2	86.1	28.5	77.0	62.0	79.0	72.5
GCRF [34]	85.2	43.9	83.3	65.2	68.3	89.0	82.7	85.3	31.1	79.5	63.3	80.5	73.2
DPN [25]	87.7	59.4	78.4	64.9	70.3	89.3	83.5	86.1	31.7	79.9	62.6	81.9	74.1
Piecewise [22]	90.6	37.6	80.0	67.8	74.4	92.0	85.2	86.2	39.1	81.2	58.9	83.8	75.3
ResNet38 [37]	94.4	72.9	94.9	68.8	78.4	90.6	90.0	92.1	40.1	90.4	71.7	89.9	82.5
PSPNet [41]	91.8	71.9	94.7	71.2	75.8	95.2	89.9	95.9	39.3	90.7	71.7	90.5	82.6
DANet [13]	—	—	—	—	—	—	—	—	—	—	—	—	82.6
DFN [38]	—	—	—	—	—	—	—	—	—	—	—	—	82.7
EncNet [40]	94.1	69.2	96.3	76.7	86.2	96.3	90.7	94.2	38.8	90.7	73.3	90.0	82.9
SANet(ours)	95.1	65.9	95.4	72.0	80.5	93.5	86.8	94.5	40.5	93.3	74.6	94.1	83.2 ¹

¹ <http://host.robots.ox.ac.uk:8080/anonymous/13JDOD.html>

Table 5: Class-wise IoUs and mIoU of PASCAL VOC dataset without pretraining on COCO dataset. The SANet achieves 83.2% mIoU that outperforms other models and dominates multiple classes. The best two entries of each column are highlighted. To make a fair comparison, models use extra datasets (e.g. JFT) are not included like [6, 27, 35, 8].

Model	Backbone	mIoU
CRF-RNN[43]		74.4
BoxSup[10]		75.2
DilatedNet[39]		75.3
DPN[25]		77.5
PieceWise[22]		78.0
Deeplab-v2[5]	ResNet101	79.7
RefineNet[21]	ResNet152	84.2
PSPNet[41]	ResNet101	85.4
DeeplabV3[5]	ResNet101	85.7
EncNet[40]	ResNet101	85.9
DFN[38]	ResNet101	86.2
SANet (ours)	ResNet101	86.1 ²

² <http://host.robots.ox.ac.uk:8080/anonymous/LCJPGE.html>

Table 6: Mean intersection over union (%) results on PASCAL VOC dataset with pretraining on COCO dataset. The SANet achieves 86.1% mIoU that is comparable results to state-of-the-art models.

and tv monitor. This result validates the effectiveness of the dual-usage SA modules. Models [9, 6] use extra datasets like JFT [32] other than PASCAL VOC or COCO are not included in Table 5.

Then, we test the SANet with COCO pretraining. As shown in Table 6, the SANet achieves an evaluated result of 85.4% mIoU using COCO data for pretraining, which is comparable to top-ranking models including PSPNet [41], and outperforms the RefineNet [21] that is built on a heavy

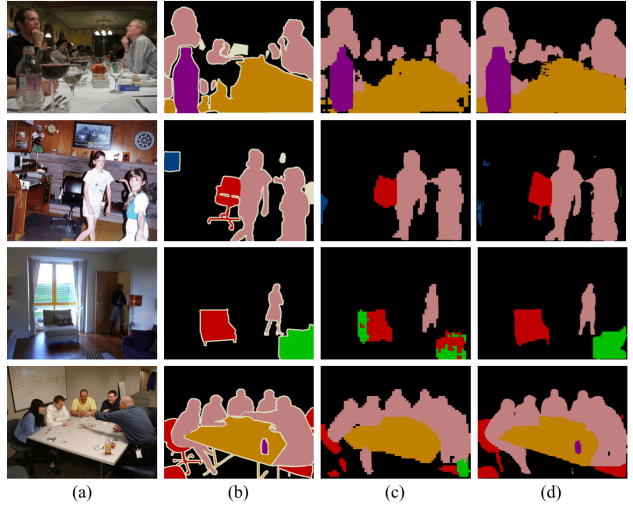


Figure 7: Example of semantic segmentation results on PASCAL VOC validation set. (a) Raw images. (b) Ground truth images. (c) FCN baseline. (d) A SANet. SANet generates more accurate parsing results compared to the baseline.

ResNet152 backbone. Our SA module is more computationally efficient than the encoding module of EncNet [40]. As shown in Fig. 6, the prediction of SANets yields clearer boundaries and better qualitative results compared to those of the baseline model. Figures 8-9 show some segmentation results on the PASCAL Context and PASCAL VOC datasets using trained SANets with ResNet101 as their backbones.

5. Conclusion

In this paper, we disentangle semantic segmentation into three tasks — categorical recognition, pixel-wise dense prediction, and pixel-group attention modeling. We design a SA module that enhances the pixelwise prediction and emphasizes the largely ignored pixel-group attention. We propose SANets to aggregate multi-stage multi-scale extracted features, resulting in promising performance. Most importantly, the SANet using EffNet-b7 sets new records on the PASCAL Context dataset. We hope that the simple yet effective SA modules and the SANets built on top of SA modules can facilitate the segmentation research of other groups.

References

[1] A. Arnab, S. Jayasumana, S. Zheng, and P. H. Torr. Higher order conditional random fields in deep neural networks. In *European Conference on Computer Vision*, pages 524–540. Springer, 2016. [2](#) [6](#)

[2] V. Badrinarayanan, A. Kendall, and R. Cipolla. Segnet: A deep convolutional encoder-decoder architecture for image segmentation. *arXiv preprint arXiv:1511.00561*, 2015. [1](#) [2](#)

[3] Y. Boykov and G. Funka-Lea. Graph cuts and efficient nd image segmentation. *International journal of computer vision*, 70(2):109–131, 2006. [1](#)

[4] Y. Boykov and V. Kolmogorov. An experimental comparison of min-cut/max-flow algorithms for energy minimization in vision. *IEEE Transactions on Pattern Analysis & Machine Intelligence*, (9):1124–1137, 2004. [1](#)

[5] L.-C. Chen, G. Papandreou, I. Kokkinos, K. Murphy, and A. L. Yuille. Deeplab: Semantic image segmentation with deep convolutional nets, atrous convolution, and fully connected crfs. *IEEE transactions on pattern analysis and machine intelligence*, 40(4):834–848, 2018. [1](#) [2](#) [3](#) [6](#) [8](#)

[6] L.-C. Chen, G. Papandreou, F. Schroff, and H. Adam. Rethinking atrous convolution for semantic image segmentation. *arXiv preprint arXiv:1706.05587*, 2017. [8](#)

[7] L.-C. Chen, Y. Yang, J. Wang, W. Xu, and A. L. Yuille. Attention to scale: Scale-aware semantic image segmentation. In *Proceedings of the IEEE conference on computer vision and pattern recognition*, pages 3640–3649, 2016. [1](#) [3](#)

[8] L.-C. Chen, Y. Zhu, G. Papandreou, F. Schroff, and H. Adam. Encoder-decoder with atrous separable convolution for semantic image segmentation. *arXiv preprint arXiv:1802.02611*, 2018. [2](#) [8](#)

[9] F. Chollet. Xception: Deep learning with depthwise separable convolutions. In *Proceedings of the IEEE conference on computer vision and pattern recognition*, pages 1251–1258, 2017. [8](#)

[10] J. Dai, K. He, and J. Sun. Boxsup: Exploiting bounding boxes to supervise convolutional networks for semantic segmentation. In *Proceedings of the IEEE International Conference on Computer Vision*, pages 1635–1643, 2015. [6](#) [7](#) [8](#)

[11] M. Everingham, S. A. Eslami, L. Van Gool, C. K. Williams, J. Winn, and A. Zisserman. The pascal visual object classes challenge: A retrospective. *International journal of computer vision*, 111(1):98–136, 2015. [1](#) [2](#)

[12] M. Everingham, L. Van Gool, C. K. Williams, J. Winn, and A. Zisserman. The pascal visual object classes (voc) challenge. *International journal of computer vision*, 88(2):303–338, 2010. [6](#) [7](#)

[13] J. Fu, J. Liu, H. Tian, Z. Fang, and H. Lu. Dual attention network for scene segmentation. *arXiv preprint arXiv:1809.02983*, 2018. [8](#)

[14] G. Ghiasi and C. C. Fowlkes. Laplacian pyramid reconstruction and refinement for semantic segmentation. In *European Conference on Computer Vision*, pages 519–534. Springer, 2016. [2](#)

[15] K. He, X. Zhang, S. Ren, and J. Sun. Spatial pyramid pooling in deep convolutional networks for visual recognition. *IEEE transactions on pattern analysis and machine intelligence*, 37(9):1904–1916, 2015. [1](#)

[16] K. He, X. Zhang, S. Ren, and J. Sun. Deep residual learning for image recognition. In *Proceedings of the IEEE conference on computer vision and pattern recognition*, pages 770–778, 2016. [2](#)

[17] J. Hu, L. Shen, S. Albanie, G. Sun, and A. Vedaldi. Gather-excite: Exploiting feature context in convolutional neural networks. In *Advances in Neural Information Processing Systems*, pages 9423–9433, 2018. [2](#) [3](#)

[18] J. Hu, L. Shen, and G. Sun. Squeeze-and-excitation networks. *arXiv preprint arXiv:1709.01507*, 7, 2017. [2](#) [3](#)

[19] M. Jaderberg, K. Simonyan, A. Zisserman, et al. Spatial transformer networks. In *Advances in neural information processing systems*, pages 2017–2025, 2015. [3](#)

[20] D. Lin, Y. Ji, D. Lischinski, D. Cohen-Or, and H. Huang. Multi-scale context intertwining for semantic segmentation. In *Proceedings of the European Conference on Computer Vision (ECCV)*, pages 603–619, 2018. [3](#)

[21] G. Lin, A. Milan, C. Shen, and I. Reid. Refinenet: Multi-path refinement networks for high-resolution semantic segmentation. In *Proceedings of the IEEE conference on computer vision and pattern recognition*, pages 1925–1934, 2017. [6](#) [8](#)

[22] G. Lin, C. Shen, A. Van Den Hengel, and I. Reid. Efficient piecewise training of deep structured models for semantic segmentation. In *Proceedings of the IEEE Conference on Computer Vision and Pattern Recognition*, pages 3194–3203, 2016. [6](#) [8](#)

[23] S. Liu, L. Qi, H. Qin, J. Shi, and J. Jia. Path aggregation network for instance segmentation. In *Proceedings of the IEEE Conference on Computer Vision and Pattern Recognition*, pages 8759–8768, 2018. [1](#)

[24] W. Liu, A. Rabinovich, and A. C. Berg. Parsenet: Looking wider to see better. 2015. [2](#) [6](#)

[25] Z. Liu, X. Li, P. Luo, C.-C. Loy, and X. Tang. Semantic image segmentation via deep parsing network. In *Proceedings of the IEEE international conference on computer vision*, pages 1377–1385, 2015. [8](#)

[26] J. Long, E. Shelhamer, and T. Darrell. Fully convolutional networks for semantic segmentation. In *Proceedings of the IEEE conference on computer vision and pattern recognition*, pages 3431–3440, 2015. [1](#) [6](#) [7](#) [8](#)

[27] P. Luo, G. Wang, L. Lin, and X. Wang. Deep dual learning for semantic image segmentation. In *Proceedings of the IEEE International Conference on Computer Vision*, pages 2718–2726, 2017. 8

[28] R. Mottaghi, X. Chen, X. Liu, N.-G. Cho, S.-W. Lee, S. Fidler, R. Urtasun, and A. Yuille. The role of context for object detection and semantic segmentation in the wild. In *Proceedings of the IEEE Conference on Computer Vision and Pattern Recognition*, pages 891–898, 2014. 6

[29] H. Noh, S. Hong, and B. Han. Learning deconvolution network for semantic segmentation. In *Proceedings of the IEEE international conference on computer vision*, pages 1520–1528, 2015. 2, 8

[30] A. Paszke, S. Gross, S. Chintala, G. Chanan, E. Yang, Z. DeVito, Z. Lin, A. Desmaison, L. Antiga, and A. Lerer. Automatic differentiation in pytorch. 2017. 6

[31] O. Ronneberger, P. Fischer, and T. Brox. U-net: Convolutional networks for biomedical image segmentation. In *International Conference on Medical image computing and computer-assisted intervention*, pages 234–241. Springer, 2015. 2

[32] C. Sun, A. Shrivastava, S. Singh, and A. Gupta. Revisiting unreasonable effectiveness of data in deep learning era. In *Proceedings of the IEEE international conference on computer vision*, pages 843–852, 2017. 8

[33] M. Tan and Q. V. Le. Efficientnet: Rethinking model scaling for convolutional neural networks. *arXiv preprint arXiv:1905.11946*, 2019. 7

[34] R. Vemulapalli, O. Tuzel, M.-Y. Liu, and R. Chellappa. Gaussian conditional random field network for semantic segmentation. In *Proceedings of the IEEE conference on computer vision and pattern recognition*, pages 3224–3233, 2016. 8

[35] G. Wang, P. Luo, L. Lin, and X. Wang. Learning object interactions and descriptions for semantic image segmentation. In *Proceedings of the IEEE Conference on Computer Vision and Pattern Recognition*, pages 5859–5867, 2017. 8

[36] X. Wang, R. Girshick, A. Gupta, and K. He. Non-local neural networks. In *Proceedings of the IEEE Conference on Computer Vision and Pattern Recognition*, pages 7794–7803, 2018. 3

[37] Z. Wu, C. Shen, and A. Van Den Hengel. Wider or deeper: Revisiting the resnet model for visual recognition. *Pattern Recognition*, 90:119–133, 2019. 8

[38] C. Yu, J. Wang, C. Peng, C. Gao, G. Yu, and N. Sang. Learning a discriminative feature network for semantic segmentation. In *Proceedings of the IEEE Conference on Computer Vision and Pattern Recognition*, pages 1857–1866, 2018. 8

[39] F. Yu and V. Koltun. Multi-scale context aggregation by dilated convolutions. *arXiv preprint arXiv:1511.07122*, 2015. 8

[40] H. Zhang, K. Dana, J. Shi, Z. Zhang, X. Wang, A. Tyagi, and A. Agrawal. Context encoding for semantic segmentation. In *The IEEE Conference on Computer Vision and Pattern Recognition (CVPR)*, 2018. 1, 2, 4, 5, 6, 8

[41] H. Zhao, J. Shi, X. Qi, X. Wang, and J. Jia. Pyramid scene parsing network. In *IEEE Conf. on Computer Vision and Pattern Recognition (CVPR)*, pages 2881–2890, 2017. 1, 2, 3, 4, 5, 6, 8

[42] H. Zhao, Y. Zhang, S. Liu, J. Shi, C. Change Loy, D. Lin, and J. Jia. Psanet: Point-wise spatial attention network for scene parsing. In *Proceedings of the European Conference on Computer Vision (ECCV)*, pages 267–283, 2018. 3

[43] S. Zheng, S. Jayasumana, B. Romera-Paredes, V. Vineet, Z. Su, D. Du, C. Huang, and P. H. Torr. Conditional random fields as recurrent neural networks. In *Proceedings of the IEEE international conference on computer vision*, pages 1529–1537, 2015. 2, 3, 6, 8

[44] B. Zhou, H. Zhao, X. Puig, S. Fidler, A. Barriuso, and A. Torralba. Scene parsing through ade20k dataset. In *Proceedings of the IEEE conference on computer vision and pattern recognition*, pages 633–641, 2017. 2

[45] B. Zhou, H. Zhao, X. Puig, T. Xiao, S. Fidler, A. Barriuso, and A. Torralba. Semantic understanding of scenes through the ade20k dataset. *International Journal of Computer Vision*, pages 1–20, 2016. 2